



The catalytic effect of titanium oxide based additives on the dehydrogenation and hydrogenation of milled MgH₂

D.L. Croston, D.M. Grant*, G.S. Walker

Department of Mechanical, Materials and Manufacturing Engineering, University of Nottingham, University Park, Nottingham, Nottinghamshire, NG7 2RD, United Kingdom

ARTICLE INFO

Article history:

Received 3 September 2008
Received in revised form 23 October 2009
Accepted 24 October 2009
Available online 31 October 2009

Keywords:

Energy storage materials
Metal hydrides
Sol–gel synthesis
Thermal analysis

ABSTRACT

Magnesium hydride (MgH₂) is considered to be one of the most promising options for a solid state hydrogen storage material. However, for practical use it is still imperative to find a convenient means of overcoming its slow kinetics and high stability. In this investigation, oxide materials based on TiO₂ have been prepared from alkoxide precursors using a sol–gel route. When ball milled with MgH₂, the titanium oxide based additives were found to result in significantly reduced onset temperatures of dehydrogenation and increased hydrogenation and dehydrogenation rates. Dehydrogenation onset temperatures as low as 257 °C were observed, which is over 100 °C lower than for milled MgH₂ with no additives. In cycling experiments at 300 °C, between pressures of 1 × 10⁻² bar H₂ and 6 bar H₂, reaction rates for dehydrogenation and hydrogenation were found to be up to 15 times quicker than for milled MgH₂ with no additives. The Ti based oxide additives were found to change the mechanism of dehydrogenation from milled MgH₂ from one of surface control followed by contracting volume, to a two-dimensional Johnson–Mehl–Avrami nucleation and growth mechanism.

© 2009 Elsevier B.V. All rights reserved.

1. Introduction

With growing concerns over pollution and global warming, hydrogen is widely accepted as an ideal non-polluting and sustainable means of delivering energy in the future, for both stationary and mobile applications. The need for a safe, cost-effective, and energy efficient means of storing hydrogen is a key issue that needs to be addressed before a practical hydrogen economy can be implemented. Storage in a solid chemical form is recognised to be safer than storage as a cryogenic liquid or compressed gas, and also it offers the highest storage capacity by volume [1]. Magnesium hydride (MgH₂) is a light, inexpensive and readily available solid storage material with a hydrogen capacity of 7.6 wt.%. Its use is unfortunately hampered by its high thermodynamic stability and its slow kinetics, requiring elevated temperatures (>400 °C) or long times (>15 h) for hydrogenation/dehydrogenation [2].

Studies have shown that the kinetics can be improved through milling [3], mechanical alloying [4,5], and addition of various additives [6], including metals [7–9], metal oxides [4,10–13], transition metal fluorides [13–16], graphite [17] and carbon nanotubes [17,18] and combinations of the above such as carbon nanotubes (CNT) and metal fluorides [19], CNT and transition metals [6]. Previous studies reported in the literature indicate that metal oxides can

have a beneficial effect on the dehydrogenation temperature and kinetics of hydrogen sorption when ball milled with Mg or MgH₂ [4,10,12,13]. The oxides used in these previous studies were generally commercial, crystalline single oxides and the mechanisms by which these oxides affect dehydrogenation and hydrogenation of MgH₂ are not yet fully understood. To our knowledge, there are no prior studies of the effect of TiO₂ prepared from an alkoxide precursor via a sol–gel route on the H₂ sorption properties of MgH₂, nor have the effects of oxide calcination temperature been previously investigated. The alkoxide sol–gel route is a well known route for producing high surface area TiO₂ and the calcination conditions can be used to control the surface area and phase of the oxide [20]. The work presented here includes results and discussion of MgH₂ milled with oxides prepared from an alkoxide precursor and calcined at temperatures from 70 °C to 800 °C. The preparation method and heat treatments give a range of titanium based oxide additives with varying bulk and surface structure, and a wide range of crystallinities and surface areas. The onset temperature and activation energy of dehydrogenation were investigated by thermogravimetric analysis (TGA) and kinetic and cycling experiments were carried out in a Hiden intelligent gravimetric analyser (IGA).

2. Experimental details

2.1. Materials preparation

Binary oxides of titanium were prepared from the precursor titanium isopropoxide (C₁₂H₂₈O₄Ti, Alfa Aesar). The required quantity of precursor for a 5 g yield of stoichiometric oxide was dissolved in 50 cm³ propan-2-ol (Fisher, analyt-

* Corresponding author. Tel.: +44 0 1159513747; fax: +44 0 1159513948.
E-mail address: david.grant@nottingham.ac.uk (D.M. Grant).

Table 1
Sample nomenclature.

Oxide calcination temperature (°C)	Sample name for oxide	Sample name for oxide milled with MgH ₂
70	Ti70	MgH ₂ -Ti70
120	Ti120	MgH ₂ -Ti120
400	Ti400	MgH ₂ -Ti400
800	Ti800	MgH ₂ -Ti800

ical grade). The slurry was hydrolysed by the addition of triply de-ionised water (TDW), using a 100% excess of TDW. After stirring for 2 h, the suspension was transferred to an evaporating dish and dried in air at 70 °C for 18 h. A portion of the dried powder was subsequently subjected to a further calcination for 2 h at 120 °C, 400 °C or 800 °C.

A rotary ball mill (Fritsch P5) was used to mill MgH₂ (*Alfa Aesar*) and MgH₂/oxide (80/20 weight ratio) mixtures under an inert argon atmosphere. A total of 5 g of powder was added to a stainless steel pot of volume 80 cm³ containing 30 stainless balls ($\varnothing = 10$ mm), giving a ball to powder weight ratio of 24:1. The mill was then run at a speed of 250 rpm for 1 h, followed by a rest for 30 min. This cycle of milling and resting was repeated to give a total milling time of 20 h.

Henceforth, the prepared oxide and MgH₂/oxide samples will be referred to using the nomenclature shown in Table 1.

2.2. Materials characterisation

Powder X-ray diffraction (XRD) patterns of the oxides were collected using a Bruker D8 diffractometer with Cu K α ($\lambda_1 = 1.54060$ Å) X-ray source operating at 40 kV and 40 mA. Diffraction patterns were collected over the 2θ range of 20°–80°, with a step size of 0.02° in 2θ and a time of 1 s per step. The Scherrer equation was used to determine average crystallite sizes of crystalline phases [21].

Surface areas of the samples were measured using the BET method with N₂ physisorption on a Quantachrome Autosorb-1 Automated Gas Sorption System. For air-sensitive samples containing MgH₂, powder was loaded into a glass sample tube inside an Ar glove box, and the top was sealed with tape, prior to removal of the tube from the glove box. The tape was removed prior to evacuation of the tube for outgassing on the Autosorb instrument.

X-ray photoelectron spectroscopy (XPS) of the MgH₂/oxide samples was carried out on a Kratos AXIS ULTRA XPS system with a monochromated Al K α X-ray source which operated at 10 mA and 15 kV and a hemispherical analyser with eight channeltrons. Samples were prepared inside an Ar glove box, by mounting powders onto double-sided tape attached to a sample bar. Samples were loaded inertly into the XPS instrument using a N₂ filled glove bag. Analysis of the XPS data was carried out using CasaXPS software (version 2.3.10). The C 1s peak at 285 eV was used for charge correction. For peak fitting, the background was corrected using a non-linear Shirley background and Gaussian/Lorentzian contributions of 30/70 were used for the fitted components.

Transmission electron microscopy (TEM) of the MgH₂/oxide samples was carried out using a JEOL FX III microscope (200 kV). Samples were prepared inside an Ar glove box, by rubbing a lacy carbon grid (300 mesh) through a small amount of powder. Samples were then mounted into the TEM transfer rod and sealed within a Perspex cover prior to removal from the glove box. The Perspex cover was removed immediately prior to transfer to the vacuum chamber of the TEM. Micrographs and selected area electron diffraction patterns were collected, and EDX was used for elemental analysis. The selected area diffraction patterns were analysed to extract the lattice spacing, d , from the crystalline samples.

Dehydrogenation of the MgH₂/oxide samples was analysed by TGA using a TA Instruments SDT600 coupled to a Hiden Analytical HPR-20 mass spectrometer. Samples (15–30 mg) were heated under flowing Ar to 600 °C at a rate of 10 °C min⁻¹. Samples heated at different heating rates of 20, 30, and 40 °C min⁻¹ were used to construct Kissinger plots to determine activation energies of dehydrogenation for certain samples.

Gravimetric analysis of the dehydrogenation and hydrogenation of the MgH₂/oxide samples was carried out using a Hiden Isochema Intelligent Gravimetric Analyser (IGA-003). Samples (50–80 mg) were loaded into stainless steel sample buckets inside the Ar glove box, and transferred to the IGA using a N₂ purged inert loader. Samples were initially dehydrided by heating for 18 h under vacuum to a temperature above the dehydrogenation onset for the given sample. Following this initial dehydrogenation, each sample was cycled 10 times between 6 bar and 1×10^{-2} bar, to complete 10 hydrogenation and dehydrogenation cycles at a constant temperature of 300 °C.

3. Results

To understand the behaviour of the prepared oxide materials when ball milled with MgH₂, the oxides and MgH₂/oxide mixtures were characterised by XRD, N₂ physisorption, TGA-MS, XPS, and TEM.

The XRD patterns of the prepared titanium oxide based materials are presented in Fig. 1, showing the amorphous structure of the samples calcined at 70 °C and 120 °C, and the anatase and rutile structures of the samples calcined at 400 °C and 800 °C, respectively. Average crystallite size of the anatase phase after calcination at 400 °C was 10 nm, and the average size of the anatase and rutile crystallites in the TiO₂ calcined at 800 °C was 250 nm and 220 nm respectively.

The surface areas of the oxides, obtained by BET, were found to have an inverse relationship with the trend in crystallite size calculated from the XRD line broadening, with the TiO₂ surface area decreasing with calcination temperature, from 455 m² g⁻¹ and 390 m² g⁻¹ at 70 °C and 120 °C, respectively, to 135 m² g⁻¹ after calcination at 400 °C, and 15 m² g⁻¹ for the sample calcined at 800 °C. This indicates sintering of the oxide particles during calcination, resulting in larger particles with a lower total surface area exposed. Ball milling of the as received MgH₂ increased the surface area of the hydride from 2 m² g⁻¹ to 10 m² g⁻¹. The introduction of the oxide additives did not further affect the milled hydride surface area, with values in the range 10–12 m² g⁻¹ for MgH₂ milled with titanium based oxide additives.

Each of the MgH₂ and MgH₂/oxide samples was analysed using a TGA-MS to measure the onset temperature of dehydrogenation, and to quantify the amount of hydrogen desorbed. Ball milling the as received MgH₂ for 20 h reduced the dehydrogenation onset temperature of the hydride from 391 °C to 360 °C. The addition of the titanium based oxide additives significantly reduced the dehydrogenation onset temperature of ball milled MgH₂, as shown by the TGA-MS traces in Fig. 2. Dehydrogenation of the MgH₂-Ti70, MgH₂-Ti120 and MgH₂-Ti400 occurred over a broad range starting at 257 °C for MgH₂-Ti70 and at 291 °C and 263 °C for MgH₂-Ti120 and MgH₂-Ti400 respectively. The dehydrogenation of MgH₂-Ti800 started at a higher temperature of 310 °C. Double peaks were observed in the MS H₂ traces of MgH₂-Ti400 and MgH₂-Ti800. Kissinger plots were constructed by plotting the natural log of heating rate over maximum peak temperature squared ($\ln(rT_p^{-2})$), against the inverse of the peak temperature (T_p^{-1}) with

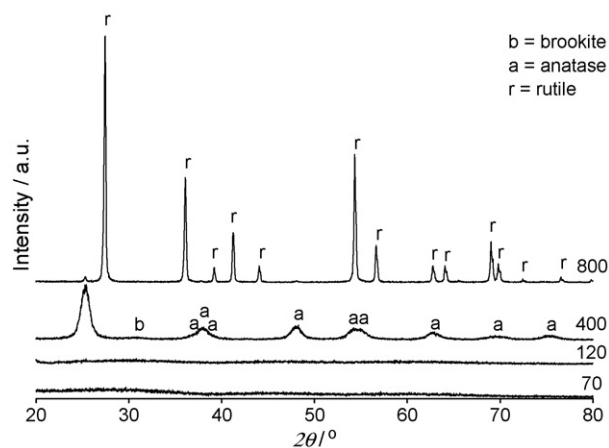


Fig. 1. XRD patterns of prepared Ti-based oxide materials after heat treatments at 70 °C, 120 °C, 400 °C and 800 °C.

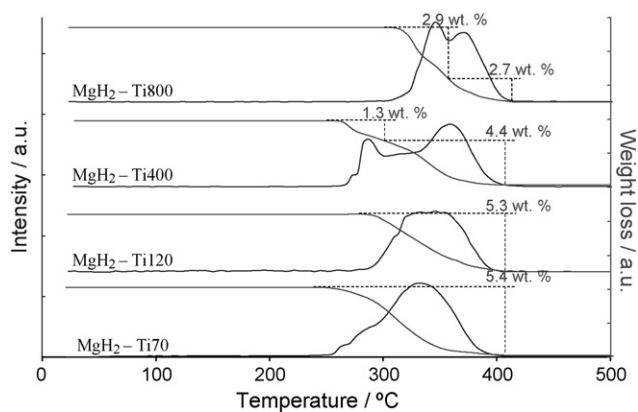


Fig. 2. TGA–MS traces of magnesium hydride and 20 wt.% titanium oxide ball milled mixtures, the oxide having been calcined at either 70 °C, 120 °C, 400 °C or 800 °C.

the data taken from TGA–MS traces at different heating rates. From these plots an activation energy of $133 \pm 20 \text{ kJ mol}^{-1}$ was calculated for milled MgH_2 and a significantly lower value of $72 \pm 3 \text{ kJ mol}^{-1}$ was determined for MgH_2 -Ti70.

Fig. 3 shows the weight loss when Ti70 is heated to 500 °C, along with the MS trace for mass 18, the water removed from the sample during heating. A loss of 23 wt.% was observed.

XPS of Ti70 and MgH_2 -Ti70 before and after dehydrogenation was carried out to examine the nature of the Ti species after milling and investigate whether there was any change in these species after dehydrogenation. XPS spectra from the Ti region of these samples are shown in Fig. 4. The Ti70 sample showed the characteristic peaks of Ti^{4+} in TiO_2 , with positions of 464.4 eV for $2p_{1/2}$ and 458.8 eV for $2p_{3/2}$. After milling and dehydrogenation, the XPS data was more difficult to collect, due to the reactive nature of the samples, their nanocrystalline structure, and the low volume fraction of TiO_2 within the samples. Short analysis times were necessary to prevent reaction of the sensitive samples whilst under the X-ray analysis beam. These short times resulted in noisy data and broadened peaks. After milling and dehydrogenation, broad peaks in the Ti 2p region were observed. Fitting of these peaks showed doublets due to titanium oxide and metallic titanium (the Ti $2p_{3/2}$ peak positions were 458.3/458.0 and 453.8/454.0, respectively). Positions of these peaks are listed in Table 2, with assignments determined from reference data, shown in Table 3 [22,23]. The relative abundance of metallic Ti increased from approximately 30% in the milled sample to approximately 40% after dehydrogenation.

TEM micrographs and associated selected area diffraction patterns collected from MgH_2 -Ti70 before and after dehydrogenation are presented in Fig. 5. Prior to dehydrogenation, the sample

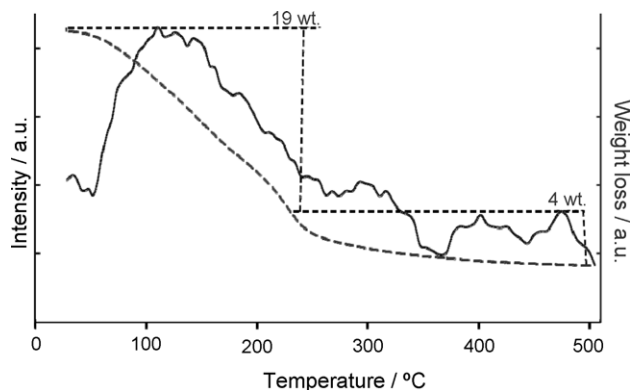


Fig. 3. Weight loss from TGA and MZ = 18 water trace for Ti70 during heating at a rate of 10 °C min^{-1} .

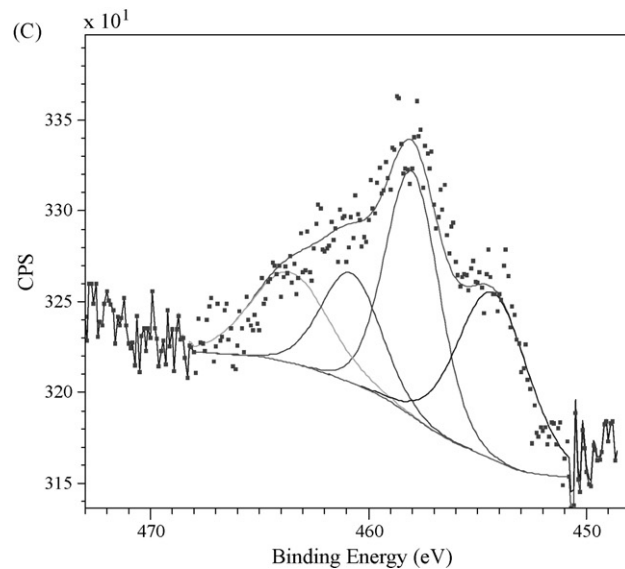
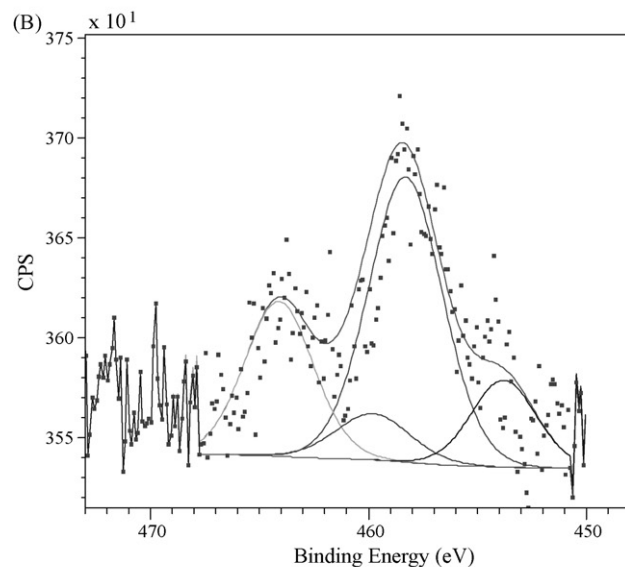
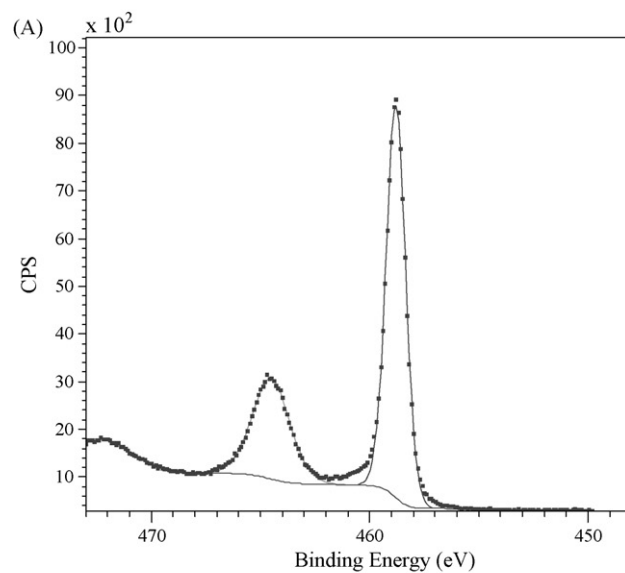


Fig. 4. XPS Ti 2p spectra from Ti70 (A), as prepared MgH_2 -Ti70 (B), and MgH_2 -Ti70 after dehydrogenation (C).

Table 2

XPS peak assignments for Ti70, as prepared MgH₂-Ti70, and MgH₂-Ti70 after dehydrogenation.

Sample	Peak position (eV)	Assignment
Ti70 before milling	464.4	Ti ^{IV} 2p _{1/2}
	458.8	Ti ^{IV} 2p _{3/2}
MgH ₂ -Ti70 after milling	464.1	Ti ^{IV} 2p _{1/2}
	458.3	Ti ^{IV} 2p _{3/2}
	459.8	Ti 2p _{1/2}
	453.8	Ti 2p _{3/2}
MgH ₂ -Ti70 after dehydrogenation	463.8	Ti ^{IV} 2p _{1/2}
	458.0	Ti ^{IV} 2p _{3/2}
	460.6	Ti 2p _{1/2}
	454.0	Ti 2p _{3/2}

Table 3

XPS Ti 2p peak positions from reference data, (a) [22] and (b) [23].

Sample	Peak assignment	Position (eV)
Ti (a)	Ti 2p _{1/2}	460.0
	Ti 2p _{3/2}	454.0
TiO (b)	Ti ^{II} 2p _{1/2}	460.2
	Ti ^{II} 2p _{3/2}	454.6
Ti ₂ O ₃ (b)	Ti ^{III} 2p _{1/2}	462.0
	Ti ^{III} 2p _{3/2}	456.8
TiO ₂ (b)	Ti ^{IV} 2p _{1/2}	464.6
	Ti ^{IV} 2p _{3/2}	458.9

appeared to consist of clusters of small particles, some of which were darker. Measuring the *d* spacing from the selected area diffraction patterns for the particles in Fig. 5(A) indicated the presence MgH₂, MgO, and anatase TiO₂. EDX analysis confirmed the presence of Mg and Ti over the whole group of particles. After dehydrogenation, the darker central particle in Fig. 5(B) appeared to be rich in Ti, with a concentration of 30 at.% from EDX quantification while the lighter bottom area was found to be 99 at.% Mg.

The gravimetric method of measuring hydrogenation and dehydrogenation was used to carry out cycling experiments to investigate the effect of repeated cycling on the kinetics of hydrogenation and dehydrogenation reactions and the overall capacity of the samples. Samples of milled MgH₂ and MgH₂-Ti70 were

Table 4

Summary of dehydrogenation onset temperatures and dehydrogenation kinetics for MgH₂ and catalysed MgH₂ samples.

Sample	Dehydrogenation onset (°C)	Dehydrogenation kinetics
Milled MgH ₂	360	90% complete in 300 min at 350 °C in 0.01 MPa H ₂
MgH ₂ -Ti70	257	90% complete in 10 min at 300 °C in 0.01 MPa H ₂
MgH ₂ -Ti120	291	n/a
MgH ₂ -Ti400	263	n/a
MgH ₂ -Ti800	310	n/a
MgH ₂ -Ti(metal)	250	90% complete in >200 min at 300 °C in 0.01 MPa H ₂

subjected to a series of 10 cycles each, between H₂ pressures of 1×10^{-2} bar and 6 bar and at a temperature of 300 °C for MgH₂-Ti70, and at 350 °C for milled MgH₂, because of the slower kinetics found for the latter. Figs. 6 and 7 present the variation of percentage reaction with respect to time for the dehydrogenation and hydrogenation of milled MgH₂, and for MgH₂-Ti70, during the first, second, third, fourth and tenth cycles. During the first dehydrogenation cycle for MgH₂, ca. 80% of the total weight loss was evolved after 12 h. For subsequent cycles, most of the weight loss, 90–95%, had occurred after 300 min (5 h). The hydrogen uptake at 350 °C and 6 bar was found to be much quicker than dehydrogenation, absorbing ca. 90% of total hydrogen in 70 min on each cycle. For MgH₂-Ti70, the first dehydrogenation took 1 h for 65% of the total H₂ to be desorbed. Subsequent dehydrogenations were found to be faster, with 90–98% of total dehydrogenation occurring in 10 min. During the hydrogenation cycles at 300 °C and 6 bar, the rate of hydrogenation of the first cycle was slower than for subsequent cycles, with only 50% of the total reaction occurring after 13 min. On the second to 10th cycles, ca. 93% of the total H₂ was absorbed by the sample in 20 min.

For comparison, a sample of MgH₂ milled with Ti metal was also prepared. A 10 wt.% addition of Ti metal (particle size <44 μm), was used, to give approximately the same wt.% of Ti as in a 20 wt.% TiO₂ addition. The results of the dehydrogenation and cycling experiments for this sample are included in the summary table, Table 4, along with all the samples reported in this work.

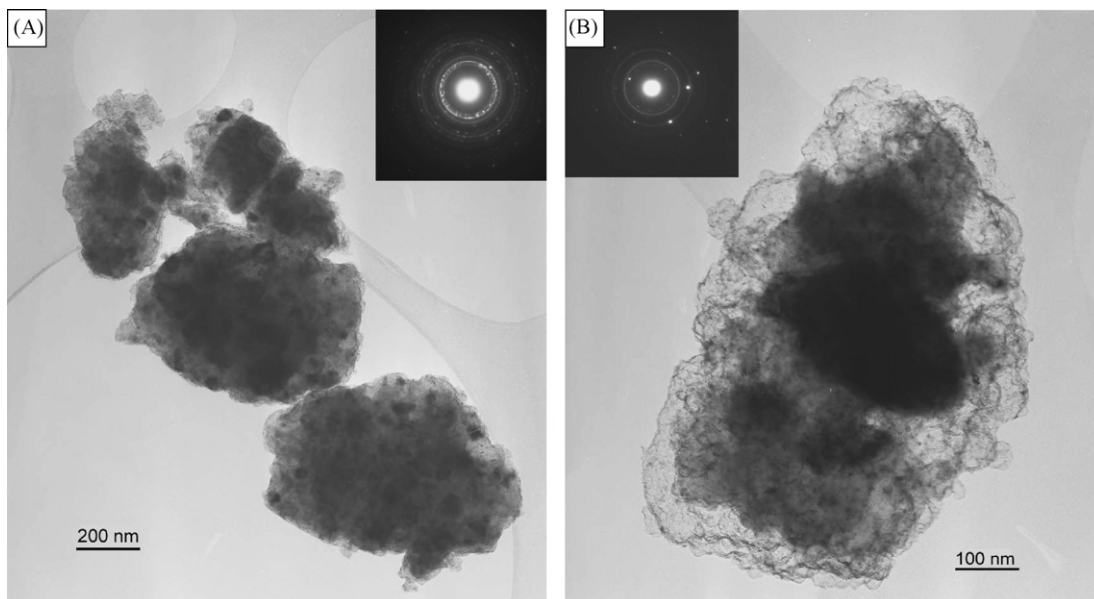


Fig. 5. TEM images and selected area diffraction patterns from as prepared MgH₂-Ti70 (A), and MgH₂-Ti70 after dehydrogenation (B).

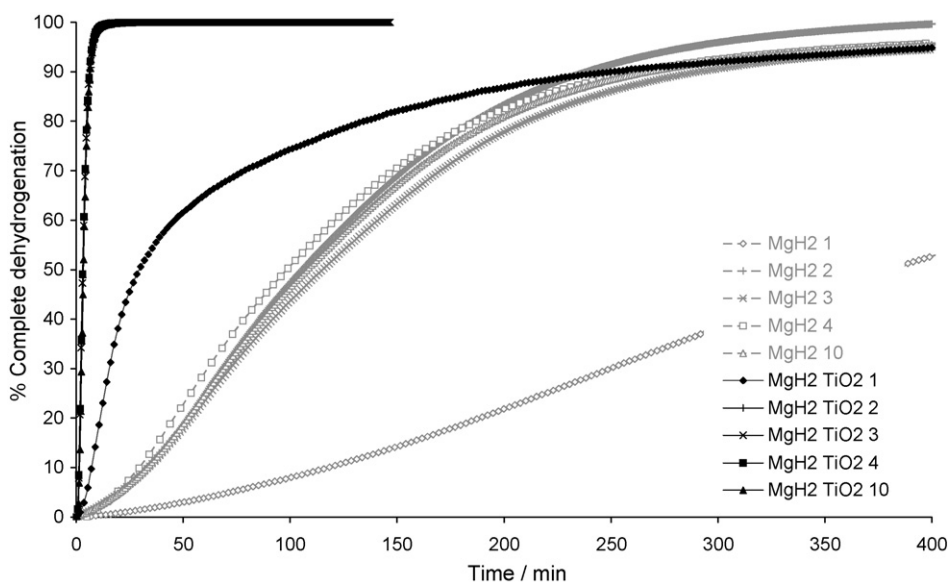


Fig. 6. Dehydrogenation of milled MgH_2 (at 350°C) and $\text{MgH}_2\text{-Ti70}$ (at 300°C) and 1×10^{-2} bar H_2 . The numbers 1, 2, 3, 4 and 10 refer to the cycle number.

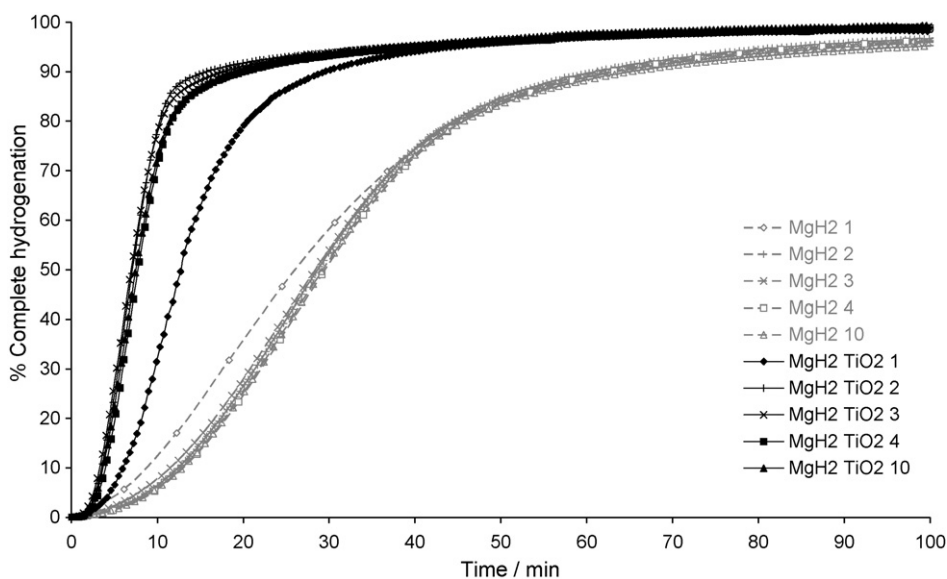


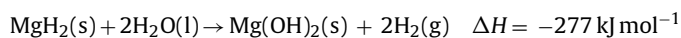
Fig. 7. Rehydrogenation of milled MgH_2 (at 350°C) and $\text{MgH}_2\text{-Ti70}$ (at 300°C) and 6 bar H_2 . The numbers 1, 2, 3, 4 and 10 refer to the cycle number.

4. Discussion

All the different TiO_2 structures have a positive effect on reducing T_{onset} of the MgH_2 , however, the amorphous structure of the oxide dried at 70°C appeared to have the greatest effect. This can be attributed to the significantly higher surface area of the lower temperature oxides. Oxides with a higher initial surface area and smaller particle size can be better dispersed within the MgH_2 during milling, and provide, therefore, a greater number of active sites for enhancing dehydrogenation. The crystalline oxide of the anatase form, Ti400, was the second most effective additive, indicating that the crystalline phases of TiO_2 have a positive effect on dehydrogenation of MgH_2 , but that their lower surface area compared to the amorphous Ti70 sample decreased their effectiveness. Amorphous Ti containing oxides have not been previously investigated, and their effect appears to be better than that of TiO_2 previously reported. A commercially available rutile form of TiO_2 additive to MgH_2 resulted in a time of 9 min for complete dehydrogenation at 350°C [10] which is a higher temperature and longer time

than reported here for the Ti70 additive. This is in agreement with the results reported here, which indicate that the amorphous Ti70 material, with its higher surface area, was more effective at enhancing dehydrogenation of MgH_2 than the crystalline anatase and rutile Ti400 and Ti800 additives.

Water reacts readily with MgH_2 via the spontaneous reaction: [24]



This reaction, occurring during the ball milling process, would result in a loss of hydrogen from the original MgH_2 starting material, and therefore a reduced H_2 capacity. For $\text{MgH}_2\text{-Ti70}$, the oxide on its own was found to lose ca. 22 wt.% of water during heating to 500°C . Assuming the reaction followed that as shown above, the reaction of this evolved water with the MgH_2 would result in a decrease in expected H_2 capacity by ca. 0.2 wt.%. Total weight loss would be expected to be higher from samples milled with oxides calcined at higher temperatures, due to the removal of water

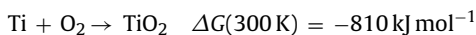
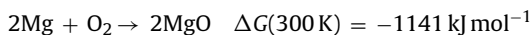
from the surface of the oxide during calcination. This was generally found to be the case, with MgH₂-Ti400 and MgH₂-Ti800 exhibiting H₂ weight losses of 5.6 wt.% and 5.7 wt.%, while MgH₂-Ti70 and MgH₂-Ti120 had lower capacities of 5.4 wt.% and 5.3 wt.% respectively. This is very close to the predicted reduction in capacity due to reaction with water from the oxides. XRD of the oxides did not show the presence of Mg(OH)₂, however, if a thin surface layer had formed on the surface of MgH₂ particles, it would have insignificant volume fraction to result in detectable diffraction lines.

XPS was used to further understand the nature of the Ti species present in the samples before and after milling and dehydrogenation. The Ti70 sample showed the characteristic peaks of Ti⁴⁺ in TiO₂, with positions of 464.4 kV for 2p_{1/2} and 458.8 kV for 2p_{3/2}. These matched well with values reported in the literature [23], shown in Table 3. After milling and dehydrogenation, broadened peaks in the Ti 2p region were observed. Milling is a very destructive high energy process resulting in the introduction of defects in the crystal structures of the materials. This leads to less structured bonding at the surface of the samples, resulting in a range of X-ray photoelectron emission energies, hence broader peaks were observed.

Fitting of the XPS data of the samples before and after dehydrogenation showed that there were two doublets corresponding to two distinct types of titanium species present in these samples. The position of the 2p_{3/2} peak of the most abundant component was 458.3 eV for the milled sample and 458.0 eV after dehydrogenation. Given the broadening of the peaks it is likely that these positions are due to TiO₂ as they match more closely to the literature value for TiO₂ than for Ti₂O₃.

The position of the 2p_{3/2} peak for the second doublet was 453.8 eV after milling, and 454.0 eV after dehydrogenation, indicating a Ti species of a lower oxidation state. These values are very close to those reported in the literature for metallic Ti [22], listed in Table 3, suggesting that complete reduction of some of the TiO₂ has occurred. The relative abundance of metallic Ti increased from approximately 30% in the milled sample to approximately 40% after dehydrogenation, indicating that TiO₂ is further reduced during dehydrogenation.

It has been suggested that Ti of a lower oxidation state than +4 can be caused by the high local temperatures arising during milling [25]. The Gibb's free energies of oxidation of Ti and Mg at 300 K are given below, showing that Ti will readily reduce at the expense of oxidation of Mg.



The same reactions could occur during dehydrogenation at elevated temperature, causing the further reduction of the Ti species observed in the XPS data after dehydrogenation.

As the hydrogenation and dehydrogenation rates improve over the first few cycles, it is likely that further reduction of the TiO₂ occurred during this period resulting in more active metal Ti species being formed. In previous reports on the behaviour of Nb₂O₅ milled with MgH₂, it was proposed that it was a sub-oxide of the form Nb₂O_{3.67}, and not a metallic Nb species, that was active in promoting the dehydrogenation of MgH₂ [26].

In order to further confirm the metallic Ti species as the active component in the dehydrogenation and hydrogenation reactions of MgH₂, a sample of MgH₂ ball milled with titanium metal rather than titanium oxide, was prepared and characterised. Metallic Ti has previously been reported as an effective catalyst for the sorption of hydrogen in MgH₂ with fast kinetics of 5 min for complete dehydrogenation at 300 °C, although details of the Ti particle size and dispersion were not included [27]. The dehydrogenation onset

temperature of the MgH₂-Ti (metal) sample prepared in the current investigation was found to be 250 °C. This is only a few degrees lower in temperature than the lowest of the MgH₂-TiO₂ samples studied, and suggests that metallic Ti is slightly more effective than TiO₂ at lowering the activation energy barrier for dehydrogenation of MgH₂. The rate of hydrogenation and dehydrogenation from the MgH₂-Ti(m) sample did not improve upon cycling, and remained slow, requiring >200 min to reach 90% of full dehydrogenation, even after 10 cycles, compared to 6 min for MgH₂-Ti70. The principle reason for the slow kinetics with the addition of metallic Ti is most likely to be due to the initial large particle size of the additive resulting in poor dispersion throughout the MgH₂. The cycling experiments showed that adding the active Ti species as a component of TiO₂, which was then reduced upon ball milling and during initial cycles between 6 bar and 1 × 10⁻³ bar H₂ at 300 °C, was a more effective way of introducing Ti to the system.

The explanation for the effectiveness of the anatase crystal structure of TiO₂ compared to the rutile form in aiding the dehydrogenation of MgH₂, relates to the reduction of the TiO₂ forming the active species. The reason for anatase TiO₂ appearing to be more effective is likely to relate to the ease of its reduction resulting in the formation of the metallic Ti species. Reports in the literature suggest that the mechanisms and rates of the reduction of rutile and anatase TiO₂ are very similar [28]. The much lower surface area of the rutile sample prepared in this study means that on a mass basis, the anatase, having more exposed surface per unit mass, loses more oxygen and is thus more effective at enhancing the dehydrogenation of MgH₂. The apparent two-step dehydrogenations observed in the TGA-MS traces for MgH₂-Ti400 and MgH₂-Ti800 is attributed to the milling efficiency for these larger TiO₂ particles (compared with the lower temperature calcined samples), leading to more heterogeneous dispersion of the TiO₂ through the MgH₂.

The activation energy values determined from TGA-MS experiments using a range of heating rates, indicated that the MgH₂-Ti70 had a significantly lower activation energy than milled MgH₂, indicating that the presence of the Ti70 lowered the activation energy barrier for the dehydrogenation of the samples. The activation energy of 133 ± 20 kJ mol⁻¹ for milled MgH₂ is consistent with reported values of 120–142 kJ mol⁻¹ [3,29–31]. There are no previously reported values of activation energies for the dehydrogenation of MgH₂ with TiO₂, however, the value of 72 ± 3 kJ mol⁻¹ is comparable with values reported for additions of Nb₂O₅, i.e. 63–83 kJ mol⁻¹ [32–34]. For metallic additions, an activation energy of 94 kJ mol⁻¹ was reported for MgH₂ milled with Ni [7].

A number of kinetic models are available to attempt to explain the complex mechanisms of dehydrogenation from MgH₂ and MgH₂ with oxide additions. Barkhordarian et al. described a range of possible models, which they applied to hydrogenation and dehydrogenation data from samples of MgH₂-Nb₂O₅ [35]. These models have been applied to the dehydrogenation data collected from the gravimetric analysis of the milled MgH₂ and MgH₂-Ti70 samples in this study. The equations for the models are given in Eqs. (1)–(5).

$$\text{SC1} \quad \alpha = kt \quad (1)$$

$$\text{JMA3} \quad [-\ln(1 - \alpha)]^{1/3} = kt \quad (2)$$

$$\text{JMA2} \quad [-\ln(1 - \alpha)]^{1/2} = kt \quad (3)$$

$$\text{CV3} \quad 1 - [1 - \alpha]^{1/3} = kt \quad (4)$$

$$\text{CV2} \quad 1 - [1 - \alpha]^{1/2} = kt \quad (5)$$

In all of the above equations, α represents the transformed fraction, k is the reaction constant, and t is the time. Eq. (1) represents a surface controlled reaction (SC1) where the recombination of hydrogen into the dihydrogen molecule at the sample surface is the rate-limiting step. Eqs. (2) and (3) are Johnson-Mehl-Avrami mod-

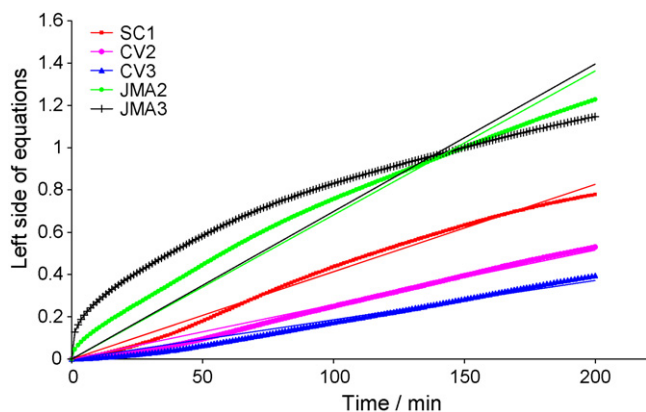


Fig. 8. Kinetic curve fitting of dehydrogenation of milled MgH_2 for $t=0$ –200 min. The y-axis is the LHS of Eqs. (1)–(5) respectively denoted by models SC1 ($R^2=0.986$), CV2 ($R^2=0.991$), CV3 ($R^2=0.978$), JMA2 ($R^2=0.942$) and JMA3 ($R^2=0.600$).

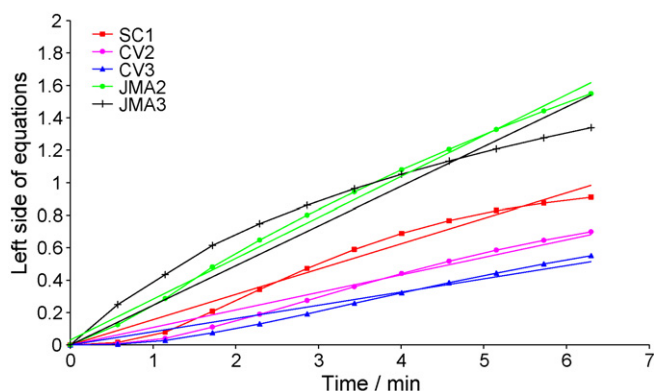


Fig. 9. Kinetic curve fitting of dehydrogenation of MgH_2 –Ti70. The y-axis is the LHS of Eqs. (1)–(5) respectively denoted by models SC1 ($R^2=0.973$), CV2 ($R^2=0.968$), CV3 ($R^2=0.956$), JMA2 ($R^2=0.993$) and JMA3 ($R^2=0.893$).

els (JMA3 and JMA2), which represent models of nucleation and growth at random points in the bulk and surface of the material. The two different equations represent two-dimensional (JMA2), and three-dimensional (JMA3) growth of nuclei. In the JMA models, the rate-limiting step is the velocity of the moving interface between the metal and the hydride. Eqs. (4) and (5) are equations for contracting volume models in which nucleation starts at the surface of the sample and then moves into the bulk, towards the core of the particle. Eqs. (4) and (5) are for three-dimensional (CV3) and two-dimensional (CV2) growth.

For the dehydrogenation data for the 5th cycle of milled MgH_2 , and MgH_2 –Ti70, the experimental data of converted fraction, α , was inserted into the left hand side of each of the kinetic Eqs. (1)–(5) and plotted against time, with linear trend lines also plotted, showing which model was the best fit to the experimental data. These plots are shown in Figs. 8–9. Linearity coefficients are listed in the figure captions to confirm the best fitting model for each set of data.

For milled MgH_2 with no additions, the experimental dehydrogenation data did not appear to fit well to one of the individual models over the full time period up to 200 min, although the closest fitting model during the later stages of dehydrogenation ($t=100$ –200 min) appeared to be the CV2 model. This model suggests the kinetics are controlled by the movement of the interface between the Mg formed at the surface of the hydride particle and the contracting hydride at the core of the particle, with two-dimensional interface growth along the grain boundaries, following the core-shell model, as proposed by Zaluska et al. [36]. A num-

ber of groups have suggested an initial surface controlled reaction for dehydrogenation of milled MgH_2 [7,37]. However, examination of the data from the early stage dehydrogenation process ($t=0$ –30 min) did not allow differentiation between the SC1 surface controlled model, and the CV2 and CV3 models, over this time period.

For MgH_2 –Ti70, the dehydrogenation data was best represented by the JMA2 model described by Eq. (3), ($R^2=0.993$) as shown in Fig. 9. The dehydrogenation of this sample, therefore, appeared to nucleate at points on the surface and within the bulk of the hydride, with kinetics controlled by a two-dimensional growth of Mg nuclei along the grain boundaries. This is to be expected, as grain boundaries provide a lower energy route for diffusion. These results suggest that the presence of the active Ti species provided active sites within the grain boundaries for the nucleation of Mg.

Barkhordarian et al. found that the kinetics of dehydrogenation from their MgH_2 – Nb_2O_5 samples generally followed a contracting volume model of two-dimensional interface growth [35], CV2, unlike the data presented here for Ti70 additive, which was best modelled by the JMA model of two-dimensional growth of nuclei. This suggests that different mechanisms are responsible for the behaviour of these different additives. Unlike the TiO_2 additives studied here, Nb_2O_5 is generally not observed to reduce during ball milling and cycling to the same extent as TiO_2 , with no evidence of any structural transformation of the Nb_2O_5 phase in some studies where Nb_2O_5 is proposed to act as the catalyst for dehydrogenation [33,34]. A degree of reduction was suggested by Friedrichs et al. who used XPS analysis and showed a reduction in the Nb species present after cycling, and evidence of a $\text{MgNb}_2\text{O}_{3.67}$ phase in XRD taken after cycling of ball milled MgH_2 – Nb_2O_5 [26]. Nb_2O_5 has also been found to be reduced in TEM studies [15] of MgH_2 – Nb_2O_5 and in other Mg based systems such as Mg–Al [38]. In contrast, for nanoparticulate metal additives, such as Ni, the JMA model has been shown to be a good representation of the dehydrogenation kinetics [7], as was found for MgH_2 –Ti70, again suggesting reduction of the amorphous TiO_2 to Ti metal had occurred. These results explain the different mechanisms at work for Nb_2O_5 and TiO_2 , where there is strong evidence pointing towards metallic Ti as the active species in increasing the rate of MgH_2 dehydrogenation. The active Ti species would therefore appear to be located within the grain boundaries of the MgH_2 , providing nucleation sites for Mg. In contrast, for Nb_2O_5 , the oxide (or suboxide) phase is thought to be located at the surface of the MgH_2 , acting as a catalyst for dissociation or recombination of hydrogen molecules on the surface of particles [35].

5. Conclusions

Oxides formed from the alkoxide precursor titanium isopropoxide via a sol–gel route were found to be highly effective in lowering the dehydrogenation onset temperature of MgH_2 , with the single oxide TiO_2 dried at 70°C having the greatest effect, lowering the dehydrogenation onset temperature to 257°C . A key result arising from this work is the previously unreported influence of the oxide calcination temperature in changing the effect of the TiO_2 on the dehydrogenation of MgH_2 . The results suggest that the anatase form of TiO_2 is more effective at lowering the dehydrogenation onset temperature of MgH_2 than the rutile TiO_2 formed after calcination at 800°C . A reduction of the Ti^{4+} in TiO_2 to metallic Ti^0 appears to result in the formation of the active species responsible for catalysing the MgH_2 dehydrogenation reaction. Although both anatase and rutile TiO_2 reduce at similar rates, the surface area of the oxide also plays a critical role in its effect. The higher surface area of the anatase TiO_2 in MgH_2 –Ti400 resulted in a high dispersion of active sites throughout the MgH_2 , compared to the lower surface area rutile TiO_2 in MgH_2 –Ti800.

By fitting isothermal dehydrogenation data with a range of kinetic models, it was found that dehydrogenation from ball milled MgH_2 occurred via a combination of surface controlled and contracting volume models, with the rate controlled by the movement of the interface between the forming Mg and the MgH_2 at the core of a particle. Upon addition of the TiO_2 or species, the mechanism was found to change, with the data fitting a Johnson–Mehl–Avrami model of Mg nucleation within the grain boundaries and growth throughout the bulk and at the surface of the MgH_2 particles.

References

- [1] J.J. Reilly, G.D. Sandrock, *Sci. Am.* 242 (1980) 118–123.
- [2] B. Vigeohlm, J. Kjoller, B. Larsen, A.S. Pedersen, *J. Less-Common Met.* 89 (1983) 135–144.
- [3] J. Huot, G. Liang, S. Boily, A. Van Neste, R. Schulz, *J. Alloys Compd.* 293 (1999) 495–500.
- [4] J.L. Bobet, B. Chevalier, M.Y. Song, B. Darriet, *J. Alloys Compd.* 356 (2003) 570–574.
- [5] N. Hanada, T. Ichikawa, S.I. Orimo, H. Fujii, *J. Alloys Compd.* 366 (2004) 269–273.
- [6] X. Yao, G. Lu, *Chin. Sci. Bull.* 53 (2008) 2421–2431.
- [7] N. Hanada, T. Ichikawa, H. Fujii, *J. Phys. Chem. B* 109 (2005) 7188–7194.
- [8] F.C. Gennari, F.J. Castro, G. Urretavizcaya, G. Meyer, *J. Alloys Compd.* 334 (2002) 277–284.
- [9] B. Molinas, A.A. Ghilarducci, M. Melnichuk, H.L. Corso, H.A. Peretti, F. Agresti, A. Bianchin, S. Lo Russo, A. Maddalena, G. Principi, *Int. J. Hydrogen Energy* 34 (2009) 4597–4601.
- [10] W. Oelerich, T. Klassen, R. Bormann, *J. Alloys Compd.* 315 (2001) 237–242.
- [11] M. Terzieva, M. Khrussanova, P. Peshev, *Int. J. Hydrogen Energy* 16 (1991) 265–270.
- [12] G. Barkhordarian, T. Klassen, R. Bormann, *Scripta Mater.* 49 (2003) 213–217.
- [13] Y. Luo, P. Wang, L.P. Ma, H.M. Cheng, *J. Alloys Compd.* 453 (2008) 138–142.
- [14] J.W. Kim, J.P. Ahn, S.A. Jin, S.H. Lee, H.S. Chung, J.H. Shim, Y.W. Cho, K.H. Oh, *J. Power Sources* 178 (2008) 373–378.
- [15] M. Porcu, A.K. Petford-Long, J.M. Sykes, *J. Alloys Compd.* 453 (2008) 341–346.
- [16] N. Recham, V.V. Bhat, M. Kandavel, L. Aymard, J.M. Tarascon, A. Rougier, *J. Alloys Compd.* 464 (2008) 377–382.
- [17] C.X. Shang, Z.X. Guo, *J. Power Sources* 129 (2004) 73–80.
- [18] D. Chen, L. Chen, S. Liu, C.X. Ma, D.M. Chen, L.B. Wang, *J. Alloys Compd.* 372 (2004) 231–237.
- [19] Y. Luo, P. Wang, L.-P. Ma, H.-M. Cheng, *Scripta Mater.* 56 (2007) 765–768.
- [20] G.S. Walker, E. Williams, A.K. Bhattacharya, *J. Mater. Sci.* 32 (2007) 5583–5592.
- [21] B.D. Cullity, S.R. Stock, *Elements of X-ray Diffraction*, 3rd ed, Prentice Hall, 2001.
- [22] A. Ermolieff, P. Bernard, S. Marthon, P. Wittmer, *Surf. Interface Anal.* 11 (1988) 563–568.
- [23] D. Gonbeau, C. Guimon, G. Pfisterguillouzo, A. Levasseur, G. Meunier, R. Dormoy, *Surf. Sci.* 254 (1991) 81–89.
- [24] M.H. Grosjean, M. Zidoune, L. Roue, J.Y. Huot, *Int. J. Hydrogen Energy* 31 (2006) 109–119.
- [25] P. Peshev, M. Khrussanova, D. Chakarov, M. Terzieva, T. Marinova, *Mater. Res. Bull.* 24 (1989) 207–212.
- [26] O. Friedrichs, J.C. Sanchez-Lopez, C. Lopez-Cartes, T. Klassen, R. Bormann, A. Fernandez, *J. Phys. Chem. B* 110 (2006) 7845–7850.
- [27] G. Liang, J. Huot, S. Boily, A. Van Neste, R. Schulz, *J. Alloys Compd.* 292 (1999) 247–252.
- [28] J.E. Rekoske, M.A. Barteau, *J. Phys. Chem. B* 101 (1997) 1113–1124.
- [29] A. Karty, J. Grunzweiggenossar, P.S. Rudman, *J. Appl. Phys.* 50 (1979) 7200–7209.
- [30] J.S. Han, M. Pezat, J.Y. Lee, *J. Less-Common Met.* 130 (1987) 395–402.
- [31] C.M. Stander, *J. Inorg. Nucl. Chem.* 39 (1977) 221–223.
- [32] J. Huot, J.F. Pelletier, L.B. Lurio, M. Sutton, R. Schulz, *J. Alloys Compd.* 348 (2003) 319–324.
- [33] G. Barkhordarian, T. Klassen, R. Bormann, *J. Alloys Compd.* 364 (2004) 242–246.
- [34] D. Fatay, A. Revesz, T. Spassov, *J. Alloys Compd.* 399 (2005) 237–241.
- [35] G. Barkhordarian, T. Klassen, R. Bormann, *J. Alloys Compd.* 407 (2006) 249–255.
- [36] A. Zaluska, L. Zaluski, J.O. Strom-Olsen, *J. Alloys Compd.* 288 (1999) 217–225.
- [37] K. Bohmhammel, B. Christ, G. Wolf, *Thermochim. Acta* 310 (1998) 167–171.
- [38] J.C. Crivello, T. Nobuki, T. Kuji, *Int. J. Hydrogen Energy* 34 (2009) 1937–1943.